Materials & Design 228 (2023) 111819

Contents lists available at ScienceDirect

Materials & Design

journal homepage: www.elsevier.com/locate/matdes

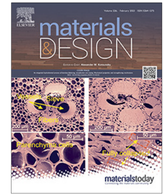

Abnormally high work hardening ability and excellent comprehensive properties of copper alloys due to multiple twins and precipitates

Yijie Ban [a,1], Meng Zhou [a,b,c,1], Yi Zhang [a,b,c,*], Yanlin Jia [d], Yong Pang [d,*], Yunzhang Li [a], Shunlong Tang [a], Xu Li [e], Alex A. Volinsky [f,g], Ekaterina S. Marchenko [g]

[a] School of Materials Science and Engineering, Henan University of Science and Technology, Luoyang 471023, PR China
[b] Provincial and Ministerial Co-construction of Collaborative Innovation Center for Non-ferrous Metal New Materials and Advanced Processing Technology, Luoyang 471023, PR China
[c] Henan Key Laboratory of Nonferrous Materials Science and Processing Technology, Luoyang 471023, PR China
[d] School of Materials Science and Engineering, Central South University, Changsha 410083, PR China
[e] Center for Advanced Measurement Science, National Institute of Metrology, Beijing 100029, PR China
[f] Department of Mechanical Engineering, University of South Florida, 4202 E. Fowler Ave. ENG030, Tampa 33620, USA
[g] Laboratory of Superelastic Biointerfaces, National Research Tomsk State University, 36 Lenin Ave., Tomsk 634050, Russia

HIGHLIGHTS

- Multiple twins give the alloy higher work hardening ability.
- The synergistic effect of multiple mechanisms gives the alloy excellent comprehensive properties.
- The ultra-low lattice mismatch between the matrix and the precipitates ensures the ductility.

GRAPHICAL ABSTRACT

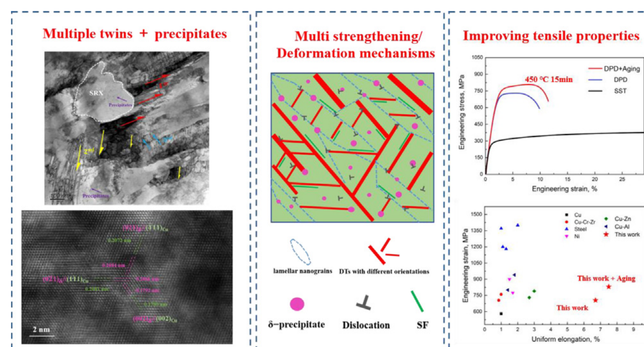

ARTICLE INFO

Article history:
Received 5 December 2022
Revised 27 February 2023
Accepted 9 March 2023
Available online 11 March 2023

Keywords:
Copper alloy
Multiple twins
Precipitates
Aging
Work hardening rate

ABSTRACT

In the present work, the Cu-1.35Ni-1Co-0.55Si alloy with multiple twins and ultra-low interfacial mismatch precipitates was obtained by liquid nitrogen dynamic plastic deformation (DPD) and aging treatment. It has abnormally high work hardening ability, which is more than twice that of the previous DPD treatment without aging. In addition, it has excellent comprehensive properties, and its strength, electrical conductivity, and elongation are 816.4 MPa, 40.2% IACS and 11.3% respectively. The fine multiple twins do not coarsen significantly during peak aging, and the dispersed nano precipitates (~3 nm) further enhance the strength of the Cu-Ni-Co-Si alloy. In addition, the low interfacial mismatch strain between the precipitates and the matrix also ensures adequate elongation. The Cu-Ni-Co-Si alloy has high strength, electrical conductivity, and ductility under the simultaneous action of various mechanisms (grain boundary strengthening, precipitation strengthening, dislocation strengthening and stacking faults). This strategy paves a new avenue for developing precipitation-strengthened alloys with excellent comprehensive properties.

© 2023 Published by Elsevier Ltd. This is an open access article under the CC BY-NC-ND license (http://creativecommons.org/licenses/by-nc-nd/4.0/).

* Corresponding authors at: School of Materials Science and Engineering, Henan University of Science and Technology, Luoyang 471023, PR China (Y. Zhang).
E-mail addresses: zhshgu436@163.com (Y. Zhang), thgink@126.com (Y. Pang).

[1] These authors contributed equally to this work.

https://doi.org/10.1016/j.matdes.2023.111819
0264-1275/© 2023 Published by Elsevier Ltd.
This is an open access article under the CC BY-NC-ND license (http://creativecommons.org/licenses/by-nc-nd/4.0/).

1. Introduction

The pursuit of materials with excellent comprehensive properties has been a lasting endeavor for the materials community [1,2,3,4]. Strength, electrical conductivity, and ductility are very important for copper alloys; however, these properties are often mutually exclusive [5,6,7]. At present, designing new material components or changing the structure of materials is the most effective way to improve the properties.

Grain refinement is a very effective method to improve the mechanical properties of materials. Refined grains introduce more grain boundaries (GBs), which are barriers to intragrain dislocation motion, making the material harder to deform plastically. Refining grains to the ultrafine and nano-size by equal angular extrusion and high-pressure torsion can make alloys several times stronger but usually leads to a significant loss of electrical conductivity and ductility [8,9]. Encouragingly, introducing nano-twins into materials has been proven to be one of the ways to improve the properties of alloys [1,10,11,12]. Like traditional grain boundaries (GBs), twin boundaries (TBs) can improve the strength by hindering the dislocation movement, but the resistivity of TBs is lower than traditional GBs. For example, the twins obtained by dynamic plastic deformation at liquid nitrogen temperature (LNT-DPD) can increase the tensile strength of pure copper to 610 MPa and electrical conductivity to 95% IACS [13]. In addition, nano twins with high density can cause the material to have high ductility because the TBs can provide ample room for dislocations' slip and storage. For example, twins are obtained in pure copper by pulsed electrodeposition technique increase the strength 10 times compared with the coarse-grained copper, and the elongation can reach 13% while maintaining adequate electrical conductivity [1]. Interestingly, scholars have found that the properties obtained by twins with different orientations in the material are much higher than the traditional grain refinement. For example, Zhao et al. [14] used gentle compression in liquid nitrogen to introduce twins with different orientations in hexagonal closed-packed titanium. The multiple twinning improved the yield strength by 50% and ductility by 20% at room temperature. The cryogenic properties were even better, with a 2 GPa yield strength and 100% tensile ductility before failure. An et al. [15] introduced the gradient nano-twin structure into the high-entropy alloy with ductility comparable to the cast alloy and the 375% strength of the cast alloy.

Precipitation strengthening is effective strategy to improve the properties of alloys, since the size and distribution of precipitates have a profound impact on the conductivity and elongation of alloys [16,17]. Traditionally, precipitation strengthening is considered the most effective method to strengthen alloys without significantly deteriorating their electrical conductivity [18]. However, the lattice mismatch often leads to strain localization around precipitates, which causes stress concentration in the alloy during deformation, leading to cracks at the interface between the precipitates and the matrix. This is the origin of the strength-ductility tradeoff in precipitation-hardened alloys [19]. In recent years, Jiang et al. [20] reported that when precipitates are coherent with the matrix, that is, the interface of the precipitates is almost the same as the surrounding matrix, and has an extremely low mismatch, the alloy can be strengthened without sacrificing ductility (the elongation is unchanged, and the strength is doubled).

As representative precipitation-strengthened alloys, Cu-Ni-Si alloys have been widely used in electronic and electrical industries, e.g., as semiconductor lead-frames and connector components, due to their excellent comprehensive properties [21,22]. There are many studies regarding improving the properties of Cu-Ni-Si alloys by adding alloying elements [23,24]. Liu et al. [25] obtained excellent comprehensive properties by adding Ti into the Cu-Ni-Si alloy, with a tensile strength of 702.2 MPa, an electrical conductivity of 40% IACS, and an elongation of 3.5%. Pan et al. [26] investigated the effect of the Co element on Cu-Ni-Si alloy properties and obtained the hardness of 265–290 HV and the electrical conductivity of 40.1–45.2% IACS. There is a lack of studies that introduce extensive twins into Cu-Ni-Si alloys to improve their properties, therefore, it is necessary to study their structural evolution and strengthening mechanisms. Twins were prepared in the Cu-Ni-Si alloy by the low-temperature DPD processes. From the technical point of view, DPD processes are neither difficult nor complicated, and the processing cost is low. The principle is that when the dislocation recovery kinetics of metals are effectively suppressed at a high strain rate (>10^3 s^{-1}) and/or low temperature, twinning is easy to form. Compared with other twin preparation technologies, such as electrodeposition, the DPD process has the most potential for industrial applications.

In this work, the Cu-Ni-Co-Si alloy with excellent comprehensive properties was obtained by LNT-DPD and subsequent aging. Interestingly, it was found that the Cu-Ni-Co-Si alloy obtained by LNT-DPD has an abnormally high uniform elongation of 6.7% without aging. The uniform elongation obtained by LNT-DPD is usually ~ 2% [27,28,29]. The results show that multiple twins solve the problem of low work hardening ability caused by the dynamic plastic deformation (DPD) treatment. In addition, the synergistic effects of multiple mechanisms improve the comprehensive properties of the Cu-Ni-Co-Si alloy.

2. Experimental procedures

The ingot with a nominal composition of the Cu-1.35Ni-1Co-0.55Si alloy was fabricated by the vacuum inductive melting in an induction furnace. The ingot was heated to 1,000 °C for 2 h and then extruded into a Φ 50 mm diameter cylinder using the metal profile extrusion machine. Then, the sample undergone homogenization treatment at 900 ℃ for 2 h followed by water quenching (WQ). Cylindrical samples with a diameter of 5 mm and a height of 7 mm were processed by LNT-DPD with a strain of $\varepsilon = 1.9$, $\varepsilon = \ln(L_0/L_f)$, where L_0 and L_f are the initial and final height of the deformed sample, respectively. Hopkinson pressure bar was the equipment for preparing LNT-DPD samples, and the strain rate is above 10^3 s^{-1}. Before impact, the samples need to be cooled by liquid nitrogen for 3 min. In addition, four LNT-DPD treated samples were aged for 15 min at 450 °C, 500 °C, 550 °C, and 600 °C, respectively. The corresponding schematic diagram of the experiment was shown in Fig. 1. The cross-sectional microstructure of the LNT-DPD samples was analyzed by a transmission electron microscope (TEM, FEI Tecnai G^2 F20) and a scanning electron microscopy with electron backscatter diffraction (SEM, EBSD, JSM-7800F). The samples for TEM analysis were prepared using Gatan 691 Precision Ion Polishing System. The EBSD samples were prepared by mechanical polishing followed by ion beam milling, and were tested with 0.6 μm EBSD step size. The tensile samples were cut perpendicular to the loading direction. The room temperature tensile tests were conducted using Instron-5848 at a strain rate of 10^{-3} s^{-1} with the dog-bone shape tensile samples with a gauge geometry of $5 \times 1 \times 0.5$ mm^3. The hardness tests were carried out using the TMVS-1 Digital Micro Vickers hardness tester with 0.3 kg load and 15 s dwell time. The electrical conductivity was measured using a Sigma2008 digital electrical instrument.

3. Results and discussion

3.1. Relationships between the microstructures and properties

Fig. 2(a) shows the solid solution microstructure of the Cu-Ni-Co-Si alloy, where the average grain size is about 230 μm. Fig. 2

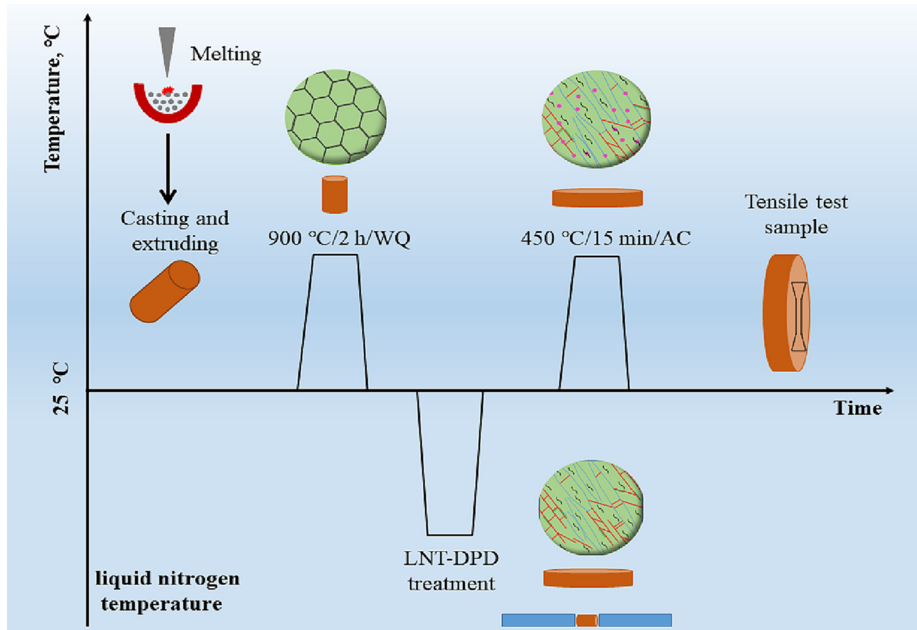

Fig. 1. Schematic of thermo-mechanical processing routes and the corresponding microstructure of the Cu-Ni-Co-Si alloy.

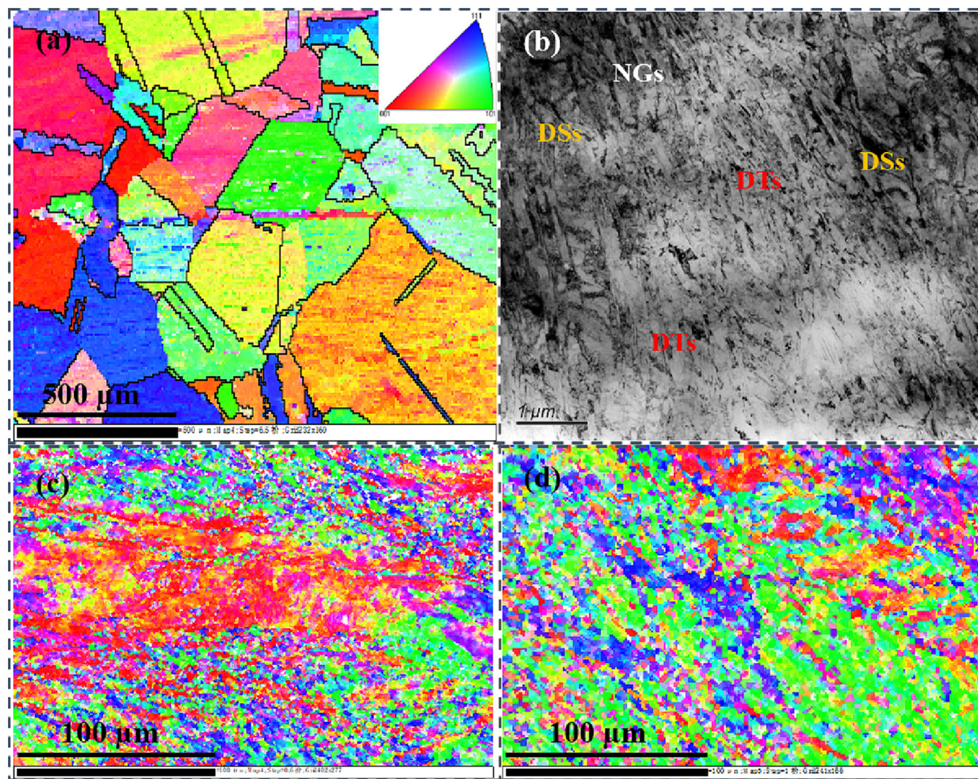

Fig. 2. Microstructures of the Cu-Ni-Co-Si alloy: (a)IPF map of solid solution state; (b) TEM image after DPD treatment; (b) IPF map after DPD treatment; (d) IPF map after DPD treatment **+** aging at 450 ℃ for 15 min.

(b) - 2 (d) shows the microstructure of the Cu-Ni-Co-Si alloy after DPD treatment. Since the grains after DPD treatment are difficult to be recognized by EBSD, the TEM image was selected for microstructure analysis. It can be seen that the Cu-Ni-Co-Si alloy after DPD treatment is composed of three structures. 1. Deformation twins (DTs) with the twin/matrix (T/M) lamellae, with an average size of 25 nm and volume fraction of 35 vol%. 2. Lamellae nanograins (NGs), with an average size of 46 nm and volume fraction of 47 vol%. 3. Dislocation entanglement and dislocation cell structure (DSs) with the size of 0.2–0.8 µm. It is worth noting that the grain size of the Cu-Ni-Co-Si alloy after DPD treatment is much smaller than pure copper after DPD treatment [30] because the addition of elements reduces the stacking fault energy (SFE) of the matrix.

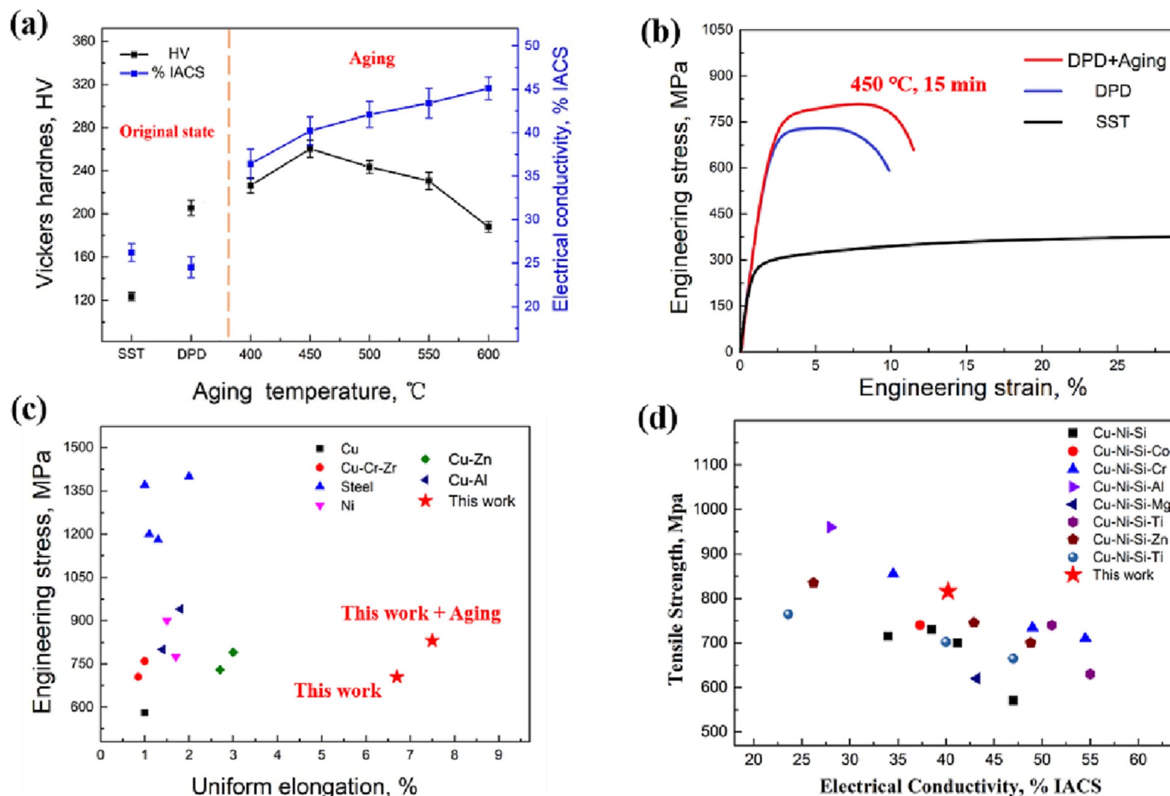

Fig. 3. (a) Hardness and electrical conductivity of the Cu-Ni-Co-Si alloy after solid solution treatment, DPD, and DPD + Aging; (b) Engineering stress–strain curves of the Cu-Ni-Co-Si alloy after solid solution treatment, DPD, and DPD + Aging; (c) Uniform elongation of different materials after DPD treatment [27,29,31,32,33,34,35,36]; (d) Tensile strength and conductivity of this work and other Cu-Ni-Si alloys [22,25,37].

The hardness and electrical conductivity of the Cu-Ni-Co-Si alloy in different states are shown in Fig. 3(a). The strength of the alloy after solid solution treatment (SST) is only 123.6 HV, and the electrical conductivity is 26.1% IACS. After DPD treatment, the hardness increased to 205.6 HV, and the electrical conductivity decreased slightly to 24.5% IACS. After aging treatment, the strength of the DPD samples reached a peak value of 260.3 HV at 450 °C for 15 min, and the conductivity was 40.2% IACS. Fig. 3(b) shows the tensile engineering stress–strain curves of the Cu-Ni-Co-Si alloy. After DPD treatment the alloy has a good tensile strength of 736.2 MPa and high uniform elongation of 6.7%, which is different from the low uniform elongation after previous DPD treatment. Fig. 3(c) shows the uniform elongation of different materials after DPD treatment. It can be seen that the uniform elongation of the material obtained by DPD treatment is usually 1–3%. In addition, the strength and elongation of the Cu-Ni-Co-Si alloy are increased after aging, i.e., 816.4 MPa and 11.3% respectively, breaking the traditional strength-elongation trade-off. In order to explain this phenomenon, the authors conducted an in-depth material characterization.

Fig. 4 shows the TEM images of the Cu-Ni-Co-Si alloy after DPD treatment. In addition to the three common structures after DPD treatment, slender multiple twins of different orientations were also found, divided into three types. 1. Twins within the T/M lamellae. The lamella of these twins is much smaller than the primary twin, with the 3–15 nm size, as seen in Fig. 4(a). 2. The multiple twins with the 6–20 nm size independently formed in the lamellar nanograins, as seen in Fig. 4(b). 3. Multiple twins with different orientations are seen in Fig. 4(c), and nano twins with different orientations labeled with different colors. The high-resolution TEM (HRTEM) further shows the characteristics of the multiple twins, as seen in Fig. 4(d). The Fast Fourier Transform (FFT) patterns corresponding to the HRTEM images of different regions in Fig. 4(d) are shown in Fig. 4d1, d2, and d3. It can be seen that in addition to extensive twins, there are also some stacking faults (SFs), and the coexistence of SFs and twins in Fig. 4(d1).

Generally, the strain hardening capability of a material is determined by the interactions between dislocations and deformation products. Although high strength is obtained after DPD treatment, the uniform elongation is low. This is due to the relatively high density of accumulated dislocations in the deformed specimen, which limits the work hardening ability of the material [38]. However, in addition to a large number of primary T/M lamellae, a wide range of multiple twins and SFs were also obtained in this work. Nano twins can offer ample room for dislocation storage, and the generation of multiple twins is more conducive to the work hardening of materials because the multiple twinning can provide adequate pathways for easy glide and cross-slip of dislocations to accommodate significant plastic deformation. In addition, the emergence of SFs also provides space for dislocation storage, which improves the work hardening rate of the Cu-Ni-Co-Si alloy [39,40]. In terms of the strength, nano twins and grain refinement can prevent the movement of dislocations to improve the strength of the alloy. Therefore, the Cu-Ni-Co-Si alloy obtained excellent strength and uniform elongation.

Fig. 5 shows the microstructure of the DPD Cu-Ni-Co-Si alloy aged at 450 °C for 15 min, which is similar to the microstructure after DPD treatment, but the grain size increases after aging. The average T/M lamella size is 35 nm, and the average nanograin size is 67 nm. Interestingly, the finer multiple twins do not seem to have changed, and the size has not increased significantly, as seen in Fig. 5(b). In addition, very few static recrystallized grains were found, which exist at the interface of twins and nanograins, where the stored energy is high and static recrystallization is easy to

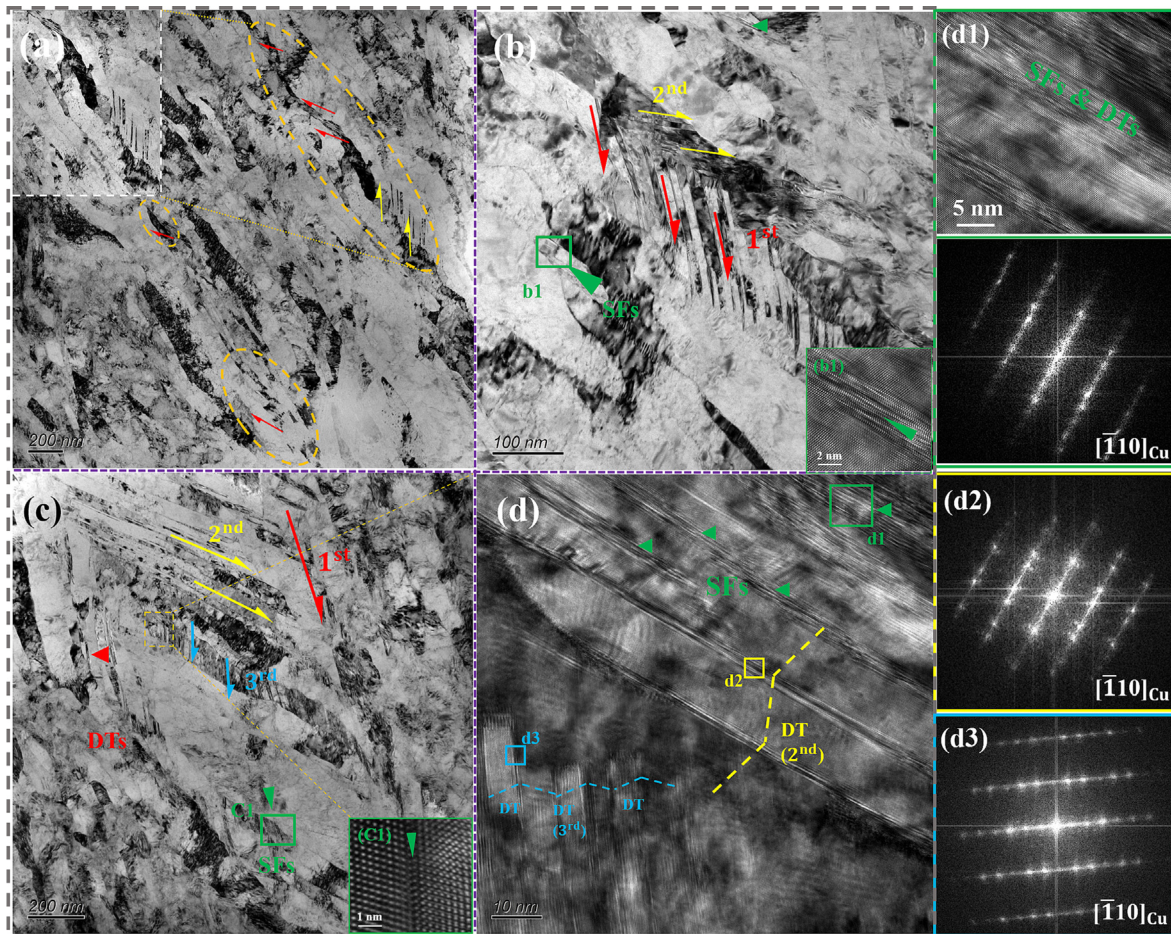

Fig. 4. TEM characterization of multiple twins in the Cu-Ni-Co-Si alloy: (a) Multiple twins in the T/M lamellae; (b) Multiple twins formed in the lamellar nanograins; (b1) Profuse SFs nano-bundles along with the corresponding HRTEM; (c) Multiple twins; (c1) Profuse SFs nano-bundles along with the corresponding HRTEM; (d) HRTEM of multiple twins and stacking faults (SFs); (d1) The SFs plus nano twins and the corresponding fast Fourier transform (FFT) pattern; (d2) and (d3) The FFT pattern corresponding to the multiple twins with different orientations in (d). For interpretation of the references to color in this figure legend, the reader is referred to the web version of this article.

nucleate. At the same time, a large number of δ-(Ni, Co)$_2$Si nano precipitates appear after aging. Fig. 5(c) shows the distribution of precipitates. The precipitates are widely and evenly distributed on the matrix and grain boundaries with a 3 nm size. There are almost no precipitates in the nano twins because the energy provided by the interiors of the twins for the nucleation of precipitates is low. Fig. 5(d) is the HRTEM image along $[1\,1\,0]_{Cu}$ $//[\bar{1}\,00]_{\delta}$. The precipitates have a disk-like shape with a 2.5 nm diameter. Moreover, these nano precipitates are highly coherent with the Cu matrix, and no interfacial dislocations are observed. The fast Fourier transform (FFT) patterns corresponding to the HRTEM images in Fig. 5(d) are shown in Fig. 5(d1) and (d2). In addition, Fig. 5(e) shows the interface mismatch between the precipitates and the matrix, and the mismatch strain is calculated as the following. The interfacial mismatch strain of $(0\,\bar{2}\,1)_{\delta}$ and $(1\,\bar{1}\,1)_{Cu}$ is 0.72%, the interfacial mismatch strain of $(021)_{\delta}$ and $(\bar{1}\,11)_{Cu}$ is 0.57%, and the interfacial mismatch strain of $(002)_{\delta}$ and $(002)_{Cu}$ is 0.67%.

According to the tensile engineering stress–strain curves in Fig. 3(b), the strength and elongation of the Cu-Ni-Co-Si alloy after aging at 450 °C for 15 min have been further improved, which is contrary to the traditional strength-elongation trade-off. After the above analysis, this phenomenon has been reasonably explained. First, the increase in strength is attributed to the appearance of precipitates. The interaction of twins, nanograins, and precipitates increases the Cu-Ni-Co-Si alloy strength. The increase in elongation is attributed to the reduction of dislocation density after aging [9]. In addition, the low interfacial mismatch strain between the precipitates and the matrix also ensures the high elongation of the Cu-Ni-Co-Si alloy. Because the low interfacial mismatch strain between the precipitates and the matrix can avoid the accumulation of dislocations near the interface and relieve the stress concentration, which has a positive effect on improving the elongation [19,41,42]. The most important is the appearance of multiple twins, which not only ensures the strength of the material but also provides high work hardening. It is worth noting that there is no significant coarsening of the finer multiple twins after aging.

3.2. The origin of multiple twins and the interaction of different mechanisms

Multiple twins exist depending on different independent slip systems during deformation, and twins in different directions do not intersect each other in Fig. 4(c). However, most of the multiple twins depend on the grain and twin boundaries for growth, as seen in Fig. 6(a) and (b). Fig. 6(a) shows the twin existing in the grain, which is accompanied by the kink of multiple atomic layers. Fig. 6(b) shows the multiple twins along the DT$_1$ twin boundary. It can be seen that an atomic layer defect SF along the DT$_1$ twin boundary, and there is no numerous dislocations and kinks at the junction of DT$_1$ and SF. With the generation of a triple atomic layer twin and a wider atomic layer twin, a kink platform and numerous dislocations appear at the grain boundary junction of DT$_1$ and DT$_2$.

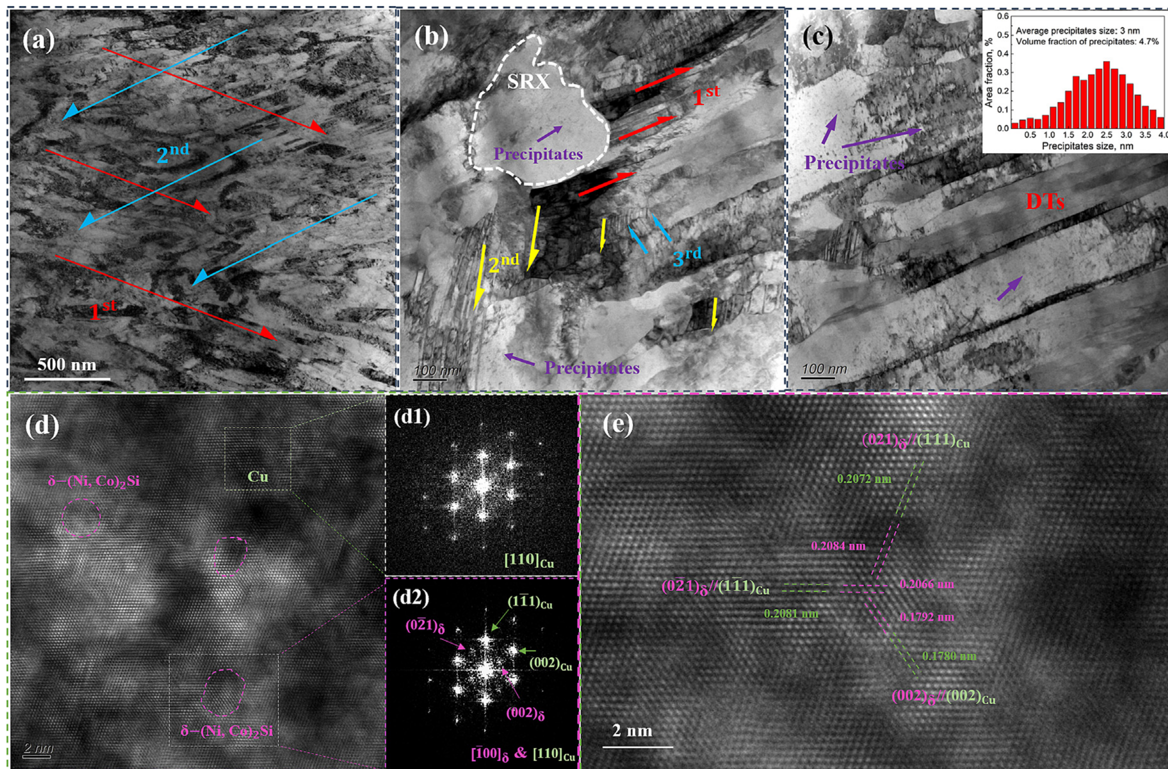

Fig. 5. TEM (HRTEM) images and corresponding FFT patterns of the Cu-Ni-Co-Si alloy aged at 450 ℃ for 15 min: (a) Bright-field TEM image; (b) Typical multiple twin structure; (c) Distribution of precipitates, and the histogram of precipitates size; (d) HRTEM image of precipitates in (c), viewed along $[110]_{Cu}//[\bar{1}00]_{\delta}$; (d1) and (d2) FFT patterns corresponding to areas outlined by green and white squares in (d), respectively; (e) Interplanar spacing between precipitates and the matrix. For interpretation of the references to color in this figure legend, the reader is referred to the web version of this article. (For interpretation of the references to color in this figure legend, the reader is referred to the web version of this article.)

It can be seen that the local lattice mismatch preexisted between the adjacent $(1\ \bar{1}\ 1)_M$ planes across the kink. The atoms near the twin boundary undergo shuffling/displacement and rearrangement under load, resulting in the nucleation and growth of DT_2 continuous nucleation along the $(11\ \bar{1})$ plane. According to the thickness of the formed DT_2 twins, the kink height is not only an important factor for the nucleation of multiple twins, but also plays a crucial role in the growth of multiple twins [43,44]. Fig. 6(b1) shows the schematic diagram of multiple twins growing along the twin grain boundary. The high kink and the occurrence of dislocation promote the nucleation and growth of multiple twins at the original grain boundary. Geometric phase analysis (GPA) analysis was conducted at the junction of multiple twins in Fig. 6(b2). It can be seen that the strain at the junction of DT_1 and DT_2 (and SF) is large, which means that the stress is concentrated in this area. The stress concentration promotes the growth of multiple twins in different directions.

These structures with multilayer SFs/DTs composite structure, and intersected DTS and DTs or SF, are vital factors for the excellent strain hardening. Specifically, besides the prevalence of single DTs and SFs, the extensive intersected and/or multi-layered nanoscale bundles of twins and/or SFs could subdivide the matrix into numerous nanoscale restricted regions. Thus, the appearance of interaction phenomenon not only facilitates microstructure refinement but also induces a Hall-Petch effect like twinning, hence leading to the increased strain hardening [45]. Moreover, according to the above analysis, it is not difficult to guess that strong interaction would occur within those intersection nodes, thereby provide more space for dislocation storage, which further confers strain hardening.

Fig. 6(c) shows the TEM micrographs of the Cu-Ni-Co-Si alloy aged at 450 °C for 15 min. In addition to the uniformly distributed precipitates in the matrix, it can be seen that the precipitates pinning twins and grain boundaries. By pinning the edge of twin tip and grain boundary, the precipitates hinder the coarsening of twin aging process, and finally make the twins have a high thermal stability. In addition, the HRTEM (Fig. 6(d)) shows that the precipitates at the grain boundary also maintain high coherence and low lattice mismatch with the matrix. The Fast Fourier Transform (FFT) patterns corresponding to the HRTEM images of different regions in Fig. 6(d) are shown in Fig. 6(d1) and (d2).

3.3. Source of excellent strength and comprehensive performance

In order to understand the strengthening effects of dynamic plastic deformation and subsequent aging of the Cu-Ni-Co-Si alloy, contributions of different strengthening mechanisms were calculated as in [46]:

$$\Delta\sigma = \Delta\sigma_0 + \Delta\sigma_P + \Delta\sigma_{GB} + \Delta\sigma_D + \Delta\sigma_{SS} \quad (1)$$

Here, $\Delta\sigma$ is the cumulative increase in strength.$\Delta\sigma_0$, $\Delta\sigma_P$, $\Delta\sigma_{GB}$, $\Delta\sigma_D$ and $\Delta\sigma_{SS}$ are contributions from Precipitation strengthening, grain boundary strengthening, dislocation strengthening and stored solution strengthening, respectively. $\Delta\sigma_0$ is the intrinsic lattice strength, which is conservatively estimated to be 52 MPa [47]. Due to that the solid solution strengthening is very limited in the Cu-Ni-Co-Si alloy, the $\Delta\sigma_{SS}$ here can be neglected [48].

For grain boundary strengthening, the strength increment can be described as:

$$\Delta\sigma_{GB} = Kd^{-1/2} \quad (2)$$

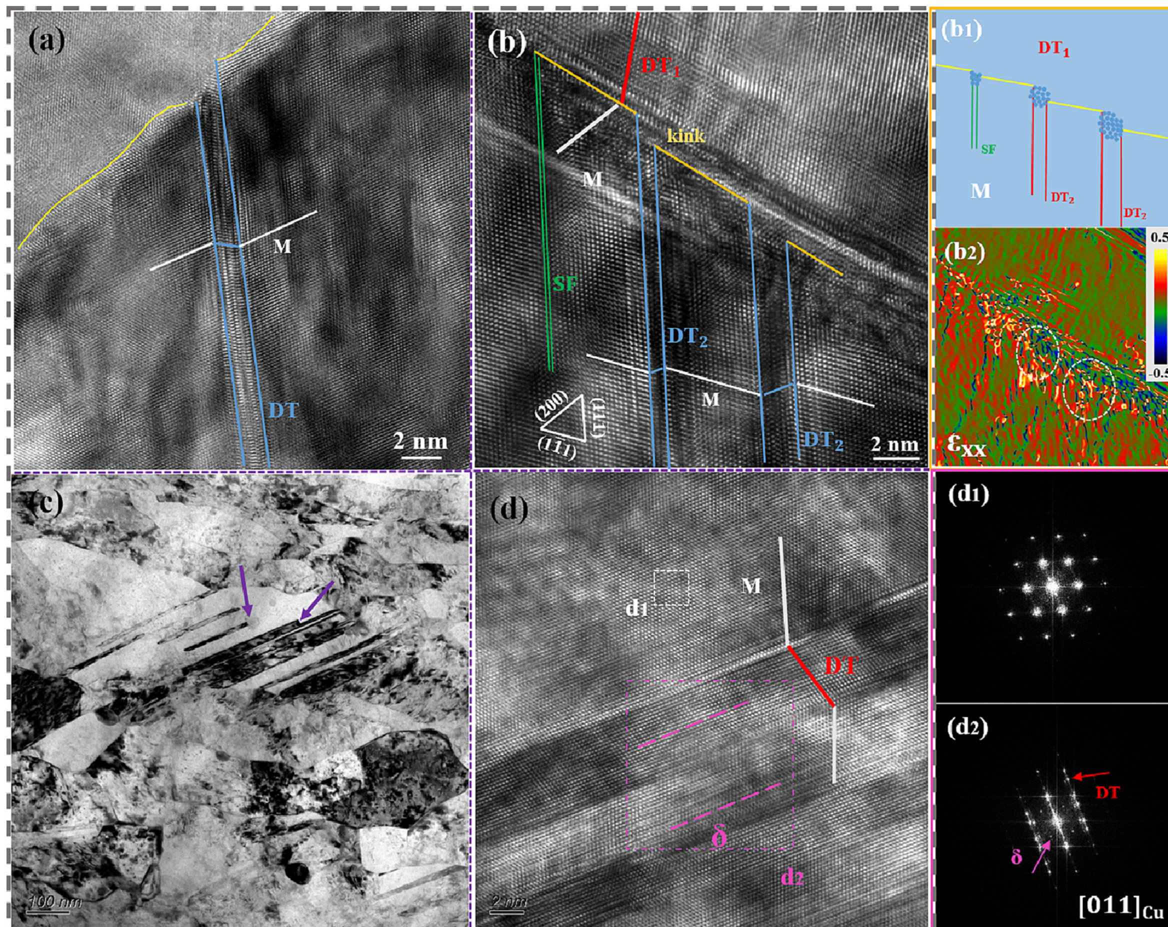

Fig. 6. Microstructure of the Cu-Ni-Co-Si alloy: (a) Deformation twin is generated along the grain boundary, and multi-layer atomic kinks occur at the tip of twins and grain boundary; (b) SF and DT_2 twins are generated along the DT_1 twin boundary, and numerous dislocations and kinks are generated at the boundary to promote the growth of DT_2 twins; (b1) The schematic diagram of multiple twins growing along the twin grain boundary; (b2) Horizontal shear strain (ε_{xx}) maps obtained via geometric phase analysis, indicating that the local stress concentration at the TB kink (marked by the white circles); (c) TEM micrographs of multiple twins and precipitates distribution; (d) High-resolution TEM image of one nanoprecipitate at a twin boundary highly coherent with the twin boundary; (d1) and (d2) FFT patterns corresponding to areas outlined by white and pink squares in (d), respectively. For interpretation of the references to color in this figure legend, the reader is referred to the web version of this article. (For interpretation of the references to color in this figure legend, the reader is referred to the web version of this article.)

Here, K is the Hall-Petch coefficient, 112 MPa·μm$^{1/2}$ [47], and d is the average grain size. The average grain size after aging at 450 ℃ for 15 min is 130 nm. The contribution from the grain boundary strengthening $\Delta\sigma_{GB}$ is around 310.8 MPa.

For dislocation strengthening $\Delta\sigma_D$, the increment of strength is related to the dislocation density. The corresponding calculation is based on the Taylor formula [22]:

$$\Delta\sigma_D = M \cdot \alpha \cdot G \cdot b \cdot \sqrt{\rho} \qquad (3)$$

Here, M is the Taylor factor, α = 0.3 is a geometric constant, G is the shear modulus, b is the Burgers vector of copper [49,50], and ρ is the dislocation density. The contribution from the dislocation strengthening $\Delta\sigma_D$ is around 213.4 MPa. Therefore, precipitation strengthening can be estimated as:

$$\Delta\sigma_P = \Delta\sigma_{Exp} - \Delta\sigma_{GB} - \Delta\sigma_D - \Delta\sigma_0 \qquad (4)$$

Here, $\Delta\sigma_{Exp}$ is the yield strength of the aged specimens measured by tensile testing. Thus, the hardening contribution caused by precipitation strengthening can be estimated as 198.8 MPa. The strengthening contribution of each factor was finally counted and shown in Fig. 7(a).

For the Cu-Ni-Si alloy, precipitation strengthening is the most important strengthening method in traditional research, and its strengthening ability usually accounts for 60% – 80% of the yield strength [22,47]. In this work, the strengthening brought by precipitation $\Delta\sigma_P$ accounted for 25.6%, the grain boundary strengthening $\Delta\sigma_{GB}$ accounted for 40.1%, and the dislocation strengthening $\Delta\sigma_D$ accounted for 27.5%. Different strengthening mechanisms play an important role in strengthening of the Cu-Ni-Si alloy. The combination of different mechanisms not only provides strength, but also ensures electrical conductivity and ductility. In addition, in order to have high strength, electrical conductivity and ductility, the method of multi-stage cold rolling **+**-multi-stage aging is usually used in the traditional research of Cu-Ni-Si alloys, which greatly affects the work efficiency. In this study, the ductility of single aging treatment was doubled while maintaining high strength (>800 MPa) and high conductivity (>40% IACS) [22]. This research provides a new way to develop Cu-Ni-Si alloy, which has excellent comprehensive properties, shortens the manufacturing process and saves energy consumption.

Based on above TEM characterization, the Schematic of microstructure of the Cu-Ni-Co-Si alloy after aging is drawn, as shown in Fig. 7(b). The high strength is mainly due to the formation of nanograin and nano twins (grain boundary strengthening), precipitation strengthening of δ particles and dislocation strengthening. The excellent elongation is due to the formation of twins and SF, which provide sufficient space for dislocation storage, and the twins with different orientations affect the slip of all slip systems [40]. In addition, the low interfacial mismatch strain between the precipitates and the matrix relieve the local stress

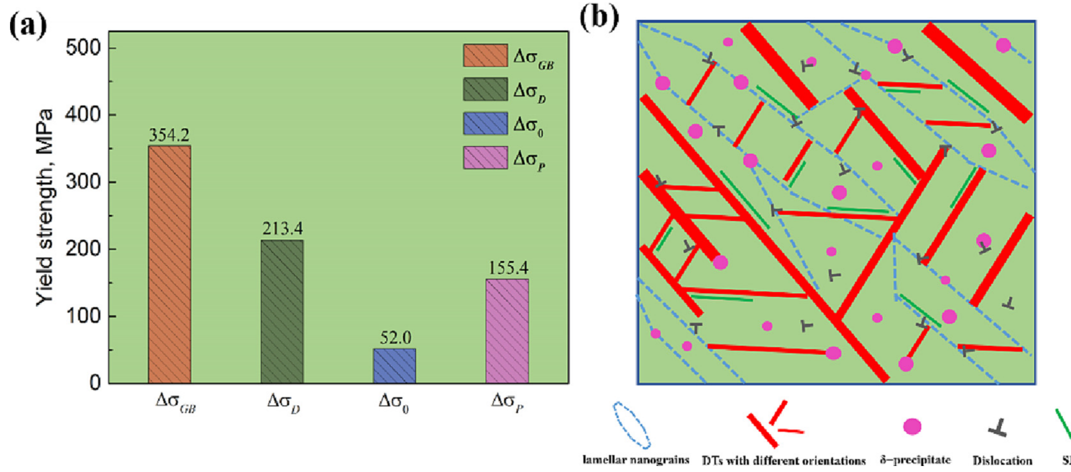

Fig. 7. (a) Strength distribution histograms of the Cu-Ni-Co-Si alloy; (b) Schematic illustration of the architected structure by the LNT-DPD and subsequent aging treatment.

concentration of the material. The Cu-Ni-Co-Si alloy has excellent comprehensive properties under the synergetic action of various mechanisms.

According to Matthiessen's rule [51], the electrical resistivity of precipitation strengthening alloy can be expressed as follow:

$$\Omega_{alloy} = \Omega_{Cu} + \Omega_{GB} + \Omega_P + \Omega_D + \Omega_{SS} \tag{5}$$

Here, Ω_{alloy} is the electrical resistivity of the aged specimen, Ω_{Cu} is the electrical resistivity of the pure Cu ($1.724 \times 10^{-8}\Omega \cdot \text{m}$ [47]),Ω_{GB}, Ω_P, Ω_D and Ω_{SS} are the resistivity increments caused by grain boundary scattering, dislocation scattering, precipitation scattering, and solute atom scattering. The resistivity of grain boundary could be expressed as:

$$\Omega_{GB} = \frac{2}{3}\Omega_{Me-GB}\left(\frac{S}{v}\right) \tag{6}$$

Here, Ω_{GB-GB} is the specific grain boundary electrical resistivity of Cu ($2.04 \times 10^{-16}\Omega \cdot \text{m}^2$), $\frac{s}{v}$ is the grain boundary area per volume, taken to be $2.37/d_{grain}$ assuming that the grains are tetrakaidecahedral [52]. d_{grain} is the average grain size. The electrical resistivity caused by grain boundaries is calculated to be $3.2 \times 10^{-9}\Omega \cdot \text{m}$. The resistivity of precipitation Ω_P can be expressed as:

$$\Omega_P = 3nf_v(\Omega_P + \Omega_{Cu}) - 3n^2 f_v{}^2 \frac{\Omega_{Ni_2Si}(\Omega_P + 3\Omega_{Cu})}{\Omega_{Cu} + 2\Omega_{Ni_2Si}} \tag{7}$$

Here, Ω_{Ni_2Si} is the electrical resistivity of Ni_2Si precipitate ($2.1 \times 10^{-7}\Omega \cdot \text{m}$ [53]), f_v is the volume fraction of $(Ni, Co)_2Si$ precipitates (~4.7% in this work) and $n = \frac{\Omega_{Ni_2Si} - \Omega_{Cu}}{2\Omega_{Ni_2Si} + \Omega_{Cu}}$. Thus, the electrical resistivity caused by precipitation can be calculated to be $5.4 \times 10^{-10}\Omega \cdot \text{m}$. The resistivity of dislocation Ω_D can be expressed as:

$$\Omega_D = p \cdot \Omega_{pd} \tag{8}$$

Here, Ω_{pd} is the specific dislocation electrical resistivity of Cu, taken to be $2 \times 10^{-25}\Omega \cdot \text{m}^3$ [47], the dislocation density increases the resistivity of the alloy by $2.4 \times 10^{-10}\Omega \cdot \text{m}$. The resistivity of solid solution Ω_{SS} can be expressed as:

$$\Omega_{SS} = \Omega_{alloy} - \Omega_{Cu} - \Omega_{GB} - \Omega_P - \Omega_D \tag{9}$$

Thus, the electrical resistivity caused by solid solution can be estimated as $1.3 \times 10^{-8}\ \Omega \cdot \text{m}$. In short, the changing trend of electrical conductivity is consistent with traditional aging and increases with aging time. This is because, with the increase of aging time, new precipitates appear and grow, which reduces the content of solute atoms in the matrix. In this work, the electrical conductivity of the Cu-Ni-Co-Si alloy at the aging peak is 40.2% IACS, which is an excellent conductivity for high-strength Cu-Ni-Si alloy [22]. Fig. 3(d) shows the comparison of conductivity between this work and other Cu-Ni-Si alloys.

In addition, this also shows that multiple twins do not significantly sacrifice conductivity to improve the strength of the alloy. However, it is not common to obtain multiple twins by DPD treatment. Therefore, more in-depth research is needed. Fortunately, the appearance of multiple twins gives the precipitation hardening alloys excellent properties. Furthermore, compared with other grain refining processes, the DPD process has a higher degree of grain refinement and is more convenient and environmentally friendly. Other technologies have a series of disadvantages, such as high processing costs, process complications, process-induced contamination or porosity, or limited kinds of processable materials. This work has obtained excellent properties by introducing twins into the alloy through DPD processes, and the process is simple and suitable for industrial applications, which provides a theoretical basis for the development of Cu-Ni-Si alloy in the future.

4. Conclusion

In summary, the Cu-Ni-Co-Si alloy with high strength, electrical conductivity, and ductility was prepared by the LNT-DPD treatment and subsequent aging. The strength is 816.4 MPa, electrical conductivity is 40.2% IACS and elongation is 11.3%. Different from the previous Cu-Ni-Co-Si alloys where precipitation strengthening was the main mechanism, various strengthening mechanisms have played an important role in this work. Various mechanisms of grain boundary, precipitation, dislocation, and SF strengthening not only increase mechanical strength but also ensure electrical conductivity and ductility. The excellent strength is attributed to the refinement of grains (twins, nanograins) and the appearance of precipitates. The high work hardening ability is attributed to multiple twins with different orientation and the low interfacial mismatch strain between the precipitates and the matrix. In addition, the finer multiple twins have no significant coarsening after peak aging.

Data availability

No data was used for the research described in the article.

Declaration of Competing Interest

The authors declare that they have no known competing financial interests or personal relationships that could have appeared to influence the work reported in this paper.

Acknowledgments

This work was supported by the National Natural Science Foundation of China (52071134), Outstanding Talents Innovation Fund of Henan Province (ZYQR201912164), the Program for Innovative Research Team at the University of the Henan Province (22IRTSTHN001), China Postdoctoral Science Foundation (2020 M682316,2021 T140779) and Special Research and Development Project of Henan Academy of Sciences (220910009).

References

[1] L. Lu, Y.F. Shen, X.H. Chen, L.H. Qian, K. Lu, Ultrahigh Strength and High Electrical Conductivity in Copper, Science 304 (2004) 422–426, https://doi.org/10.1126/science.1092905.
[2] D. Raabe, C.C. Tasan, E.A. Olivetti, Strategies for improving the sustainability of structural metals, Nature 575 (2019) 64–74, https://doi.org/10.1038/s41586-019-1702-5.
[3] K. Lu, L. Lu, S. Suresh, Strengthening materials by engineering coherent internal boundaries at the nanoscale, Science 324 (2009) 349–352, https://doi.org/10.1126/science.1159610.
[4] Y.F. Shen, L. Lu, Q.H. Lu, Z.H. Jin, K. Lu, Tensile properties of copper with nano-scale twins, Scr. Mater. 10 (2005) 989–994, https://doi.org/10.1016/j.scriptamat.2005.01.033.
[5] D.W. Callister Jr, Materials Science and Engineering, An Introduction, USA, 2000.
[6] Y.M. Wang, M.G. Chen, F.H. Zhou, E. Ma, High tensile ductility in a nanostructured metal, Nature 419 (2002) 912–915, https://doi.org/10.1038/nature01133.
[7] R.H. Pry, R.W. Hennig, On the use of electrical resistivity as a measure of plastic deformation in copper, Acta Metall. 318 (1954) 318–321, https://doi.org/10.1016/0001-6160(54)90174-1.
[8] A. Vinogradov, V. Patlan, Y. Suzuki, K. Kitagawa, V.I. Kopylov, Structure and properties of ultra-fine grain Cu-Cr-Zr alloy produced by equal-channel angular pressing, Acta Mater. 50 (2002) 1639–1651, https://doi.org/10.1016/S1359-6454(01)00437-2.
[9] K.S. Raju, V.S. Sarma, A. Kauffmann, Z. Hegedűs, J. Gubicza, M. Peterlechner, J. Freudenberger, G. Wilde, High strength and ductile ultrafine-grained Cu-Ag alloy through bimodal grain size, dislocation density and solute distribution, Acta Mater. 61 (2013) 228–238, https://doi.org/10.1016/j.actamat.2012.09.053.
[10] Y.T. Zhu, X.Z. Liao, X.L. Wu, Deformation twinning in nanocrystalline materials, Prog. Mater. Sci. 57 (2012) 1–62, https://doi.org/10.1016/j.pmatsci.2011.05.001.
[11] M. Dao, L. Lu, Y.F. Shen, S. Suresh, Strength, strain-rate sensitivity and ductility of copper with nanoscale twins, Acta Mater. 54 (2006) 5421–5432, https://doi.org/10.1016/j.actamat.2006.06.06.
[12] Z.X. Wu, Y.W. Zhang, D.J. Srolovitz, Dislocation-twin interaction mechanisms for ultrahigh strength and ductility in nanotwinned metals, Acta Mater. 57 (2009) 4508–4518, https://doi.org/10.1016/j.actamat.2009.06.015.
[13] Y. Zhang, Y.S. Li, N.R. Tao, K. Lu, High strength and high electrical conductivity in bulk nano-grained Cu embedded with nano-scale twins, Appl. Phys. Lett. 91 (2007) 282–285, https://doi.org/10.1063/1.2816126.
[14] S.T. Zhao, R.P. Zhang, Q. Yu, J. Ell, R.O. Ritchie, A.M. Minor, Cryoforged nanotwinned titanium with ultrahigh strength and ductility, Science 373 (2021) 1363–1368, https://doi.org/10.1126/science.abe7252.
[15] Z.B. An, S.C. Mao, Y.N. Liu, H. Zhou, Y.D. Zhai, Z.Y. Tian, C.X. Liu, Z. Zhang, X.D. Han, Hierarchical grain size and nanotwin gradient microstructure for improved mechanical properties of a non-equiatomic CoCrFeMnNi high-entropy alloy, J. Mater. Sci. Technol. 92 (2021) 195–207, https://doi.org/10.1016/j.jmst.2021.02.059.
[16] S. Qin, M.X. Yang, P. Jiang, J. Wang, X.L. Wu, H. Zhou, F.P. Yuan, Designing structures with combined gradients of grain size and precipitation in high entropy alloys for simultaneous improvement of strength and ductility, Acta Mater. 230 (2022), https://doi.org/10.1016/j.actamat.2022.117847 117847.
[17] Y.H. Zhao, X.Z. Liao, S. Cheng, E. Ma, Y.T. Zhu, Simultaneously Increasing the Ductility and Strength of Nanostructured Alloys, Adv. Mater. 18 (2006) 2280–2283, https://doi.org/10.1002/adma.200600310.
[18] S.J. Zhang, R.G. Li, H.J. Kang, Z.N. Chen, W. Wang, C.L. Zou, T.J. Li, T.M. Wang, A high strength and high electrical conductivity Cu-Cr-Zr alloy fabricated by cryorolling and intermediate aging treatment, Mater. Sci. Eng. A 680 (2017) 108–114, https://doi.org/10.1016/j.msea.2016.10.087.
[19] H.Y. Yang, K.Q. Li, Y.Q. Bu, J.M. Wu, Y.T. Fang, L. Meng, J.B. Liu, H.T. Wang, Nanoprecipitates induced dislocation pinning and multiplication strategy for designing high strength, plasticity and conductivity Cu alloys, Scr. Mater. 195 (2021), https://doi.org/10.1016/j.scriptamat.2021.113741 113741.
[20] S.H. Jiang, H. Wang, Y. Wu, X.J. Liu, H.H. Chen, M.J. Yao, B. Gault, D. Ponge, D. Raabe, A. Hirata, M.W. Chen, Y.D. Wang, Z.P. Lu, Ultrastrong steel via minimal lattice misfit and high-density nanoprecipitation, Nature 544 (2017) 460–464, https://doi.org/10.1038/nature22032.
[21] J. Yi, Y.L. Jia, Y.Y. Zhao, Z. Xiao, K.J. He, Q. Wang, M.P. Wang, Z. Zhou, Precipitation behavior of Cu-3.0Ni-0.72Si alloy, Acta Mater. 166 (2019) 261–270, https://doi.org/10.1016/j.actamat.2018.12.047.
[22] Y.J. Ban, Y.F. Geng, J.R. Hou, Y. Zhang, M. Zhou, Y.L. Jia, B.H. Tian, Y. Liu, X. Li, A. A. Volinsky, Properties and precipitates of the high strength and electrical conductivity Cu-Ni-Co-Si-Cr alloy, J. Mater. Sci. Technol. 93 (2021) 1–6, https://doi.org/10.1016/j.jmst.2021.03.049.
[23] J.Z. Huang, Z. Xiao, J. Dai, Z. Li, H.Y. Jiang, X.X. Zhang, Microstructure and Properties of a Novel Cu-Ni-Co-Si-Mg Alloy with Super-high Strength and Conductivity, Mater. Sci. Eng. A 744 (2019) 754–763, https://doi.org/10.1016/j.msea.2018.12.075.
[24] Y.J. Ban, Y. Zhang, Y.L. Jia, B.H. Tian, A.A. Volinsky, X.H. Zhang, Q.F. Zhang, Y.F. Geng, Y. Liu, X. Li, Effects of Cr addition on the constitutive equation and precipitated phases of copper alloy during hot deformation, Mater. Des. 191 (2020), https://doi.org/10.1016/j.matdes.2020.108613 108613.
[25] Q. Liu, T.H. Wang, J. Jiao, W. Wang, H.Y. Liu, X. Zhang, C.X. Zhang, F.G. Qi, J.C. Jie, X.X. Xu, H.M. Ding, The microstructures and properties of diamond reinforced Cu-Ni-Si-Ti alloys, Mater. Sci. Eng. A 862 (2023), https://doi.org/10.1016/j.msea.2022.144478 144478.
[26] S.B. Pan, Y.J. Wang, J.X. Yu, M.J. Yang, Y.Q. Zhang, H.T. Wei, Y.C. Chao, J.W. Wu, J. J. Han, C.P. Wang, X.J. Liu, Accelerated discovery of high-performance Cu-Ni-Co-Si alloys through machine learning, Mater. Des. 209 (2021), https://doi.org/10.1016/j.matdes.2021.109929 109929.
[27] Y.S. Li, Y. Zhang, N.R. Tao, K. Lu, Effect of thermal annealing on mechanical properties of a nanostructured copper prepared by means of dynamic plastic deformation, Scr. Mater. 59 (2008) 475–478, https://doi.org/10.1016/j.scriptamat.2008.04.043.
[28] H.Z. Zhao, Z.S. You, N.R. Tao, L. Lu, Anisotropic strengthening of nanotwin bundles in heterogeneous nanostructured Cu: Effect of deformation compatibility, Acta Mater. 210 (2021), https://doi.org/10.1016/j.actamat.2021.116830 116830.
[29] Y. Zhang, N.R. Tao, K. Lu, Effects of stacking fault energy, strain rate and temperature on microstructure and strength of nanostructured Cu-Al alloys subjected to plastic deformation, Acta Mater. 59 (2011) 6048–6058, https://doi.org/10.1016/j.actamat.2011.06.013.
[30] Y.S. Li, N.R. Tao, K. Lu, Microstructural evolution and nanostructure formation in copper during dynamic plastic deformation at cryogenic temperatures, Acta Mater. 56 (2008) 230–241, https://doi.org/10.1016/j.actamat.2007.09.020.
[31] Z.Y. Zhang, L.X. Sun, N.R. Tao, Nanostructures and nanoprecipitates induce high strength and high electrical conductivity in a CuCrZr alloy, J. Mater. Sci. Technol. 48 (2020) 18–22, https://doi.org/10.1016/j.jmst.2019.12.022.
[32] F.K. Yan, G.Z. Liu, N.R. Tao, K. Lu, Strength and ductility of 316L austenitic stainless steel strengthened by nano-scale twin bundles, Acta Mater. 60 (2012) 1059–1071, https://doi.org/10.1016/j.actamat.2011.11.009.
[33] Z.P. Luo, H.W. Zhang, N. Hansen, K. Lua, Quantification of the microstructures of high purity nickel subjected to dynamic plastic deformation, Acta Mater. 60 (2012) 1322–1333, https://doi.org/10.1016/j.actamat.2011.11.035.
[34] G.H. Xiao, N.R. Tao, K. Lu, Microstructures and mechanical properties of a Cu-Zn alloy subjected to cryogenic dynamic plastic deformation, Mater. Sci. Eng. A 513 (2009) 13–21, https://doi.org/10.1016/j.msea.2009.01.022.
[35] C. Gao, Y.C. Wang, X.W. Chen, Z. Li, H.N. Cai, T.G. Langdon, Achieving an excellent combination of strength and plasticity in a low carbon steel through dynamic plastic deformation and subsequent annealing, Mater. Sci. Eng. A 842 (2022), https://doi.org/10.1016/j.msea.2022.143051 143051.
[36] L.X. Sun, N.R. Tao, M. Kuntz, J.Q. Yu, K. Lu, d Low-carbon Steel Prepared by Using Dynamic Plastic Deformation, J. Mater. Sci. Technol. 30 (2014) 731–735, https://doi.org/10.1016/j.jmst.2014.03.008.
[37] W. Wang, E.Y. Gu, Z.N. Chen, H.J. Kang, Z.J. Chen, C.L. Zou, R.G. Li, G.M. Yin, T.M. Wang, Correlation between microstructures and mechanical properties of cryorolled CuNiSi alloys with Cr and Zr alloying, Mater. Charact. 144 (2018) 532–546, https://doi.org/10.1016/j.matchar.2018.08.003.
[38] W.S. Zhao, N.R. Tao, J.Y. Guo, Q.H. Lu, K. Lu, High density nano-scale twins in Cu induced by dynamic plastic deformation, Scr. Mater. 53 (2005) 745–749, https://doi.org/10.1016/j.scriptamat.2005.05.022.
[39] Y. Ma, F.P. Yuan, M.X. Yang, P. Jiang, E. Ma, X.L. Wu, Dynamic shear deformation of a CrCoNi medium-entropy alloy with heterogeneous grain structures, Acta Mater. 148 (2018) 407–418, https://doi.org/10.1016/j.actamat.2018.02.016.
[40] S. Qu, X.H. An, H.J. Yang, C.X. Huang, G. Yang, Q.S. Zang, Z.G. Wang, S.D. Wu, Z.F. Zhang, Microstructural evolution and mechanical properties of Cu-Al alloys subjected to equal channel angular pressing, Acta Mater. 57 (2009) 1586–1601, https://doi.org/10.1016/j.actamat.2008.12.002.
[41] X.H. Du, W.P. Li, H.T. Chang, T. Yang, G.S. Duan, B.L. Wu, J.C. Huang, F.R. Chen, C. T. Liu, W.S. Chuang, Y. Lu, M.L. Sui, E.W. Huang, Dual heterogeneous structures lead to ultrahigh strength and uniform ductility in a Co-Cr-Ni medium-entropy alloy, Nat. Commun. 11 (2020) 2390, https://doi.org/10.1038/s41467-020-16085-z.
[42] S.Y. Peng, Y.J. Wei, H.J. Gao, Nanoscale precipitates as sustainable dislocation sources for enhanced ductility and high strength, P. Natl. Acad. Sci. U. S. A. 117 (2020) 5204–5209, https://doi.org/10.1073/pnas.1914615117.

[43] Q. Zhu, Q.S. Huang, Y.Z. Tian, S.C. Zhao, Y.B. Chen, G. Cao, K.X. Song, Y.J. Zhou, W. Wang, Z. Zheng, X.H. An, H.F. Zhou, J.W. Wang, Hierarchical twinning governed by defective twin boundary in metallic materials, Sci. Adv. 8 (2022) 8299, https://doi.org/10.1126/sciadv.abn8299.

[44] Y.B. Chen, S.C. Zhao, Q.S. Huang, Q. Zhu, K.X. Song, H.F. Zhou, J.W. Wang, A geometrical model for grain boundary migration mediated formation of multifold twins, Int. J. Plast. 148 (2022), https://doi.org/10.1016/j.ijplas.2021.103128 103128.

[45] S. Picak, J. Liu, C. Hayrettin, W. Nasim, D. Canadinc, K. Xie, Y.I. Chumlyakov, I.V. Kireeva, I. Karaman, Anomalous work hardening behavior of Fe40Mn40Cr10Co10 high entropy alloy single crystals deformed by twinning and slip, Acta Mater. 181 (2019) 555–569, https://doi.org/10.1016/j.actamat.2019.09.048.

[46] S. Zhang, W. Hu, R. Berghammer, G. Gottstein, Microstructure evolution and deformation behavior of ultrafine-grained Al-Zn-Mg alloys with fine η′ precipitates, Acta Mater. 58 (2010) 6695–6705, https://doi.org/10.1016/j.actamat.2010.08.034.

[47] H.W. Fu, Y.W. Yin, Y. Zhang, M.Y. Zhang, X.B. Yun, Enhancing the comprehensive properties of as-cast Cu-Ni-Si alloys by continuous extrusion combined with subsequent thermomechanical treatment, Mater. Des. 222 (2022), https://doi.org/10.1016/j.matdes.2022.111033 111033.

[48] Z.L. Zhao, Z. Xiao, Z. Li, W.T. Qiu, H.Y. Jiang, L. Qian, Z.R. Liu, Y.B. Jiang, S.J. Zhang, Microstructure and properties of a Cu-Ni-Si-Co-Cr alloy with high strength and high conductivity, Mater. Sci. Eng. A. 759 (2019) 396–403, https://doi.org/10.1016/j.msea.2019.05.003.

[49] B. Rouxel, C. Cayron, J. Boranand, P. Sanders, R.E. Loge, Micro-addition of Fe in highly alloyed Cu-Ti alloys to improve both formability and strength, Mater. Des. 213 (2022), https://doi.org/10.1016/j.matdes.2021.110340 110340.

[50] Y.F. Geng, Y.J. Ban, X. Li, Y. Zhang, Y.L. Jia, B.H. Tian, M. Zhou, Y. Liu, A.A. Volinsky, K.X. Song, Excellent mechanical properties and high electrical conductivity of Cu-Co-Si-Ti alloy due to multiple strengthening, Mater. Sci. Eng. A 821 (2021), https://doi.org/10.1016/j.msea.2021.141639 141639.

[51] D. Mattissen, D. Raabe, F. Heringhaus, Experimental investigation and modeling of the influence of microstructure on the resistive conductivity of a Cu-Ag-Nb in situ composite, Acta Mater 47 (1999) 1627–1634, https://doi.org/10.1016/S1359-6454(99)00026-9.

[52] S. Pan, J. Yuan, P. Zhang, M. Sokoluk, G. Yao, X. Li, Effect of electron concentration on electrical conductivity in in situ Al-TiB2 nanocomposites, Appl. Phys. Lett. 116 (2020), https://doi.org/10.1063/1.5129817 014102.

[53] Y.P. Song, A.L. Schmitt, J. Song, Ultralong Single-Crystal Metallic Ni2Si Nanowires with Low Resistivity, Nano Lett 7 (2007) 965–969, https://doi.org/10.1021/nl0630687.